Mar Geophys Res (2008) 29:223–238
DOI 10.1007/s11001-008-9059-4

ORIGINAL RESEARCH PAPER

Magnetic zoning and seismic structure of the South China Sea ocean basin

Chun-Feng Li · Zuyi Zhou · Jiabiao Li · Bing Chen · Jianhua Geng

Received: 6 March 2008 / Accepted: 30 November 2008 / Published online: 30 December 2008

Abstract We made a systematic investigation on major structures and tectonic units in the South China Sea basin based on a large magnetic and seismic data set. For enhanced magnetic data interpretation, we carried out various data reduction procedures, including upward continuation, reduction to the pole, 3D analytic signal and power spectrum analyses, and magnetic depth estimation. Magnetic data suggest that the South China Sea basin can be divided into five magnetic zones, each with a unique magnetic pattern. Zone A corresponds roughly to the area between Taiwan Island and a relict transform fault, zone B is roughly a circular feature between the relict transform fault and the northwest sub-basin, and zones C, D, and E are the northwest sub-basin, the east sub-basin, and the southwest sub-basin, respectively. This complexity in basement magnetization suggests that the South China Sea evolved from multiple stages of opening under different tectonic settings. Magnetic reduction also fosters improved interpretation on continental margin structures, such as Mesozoic and Cenozoic sedimentary basins and the offshore south China magnetic anomaly. We also present, for the first time, interpretations of three new 2D reflection seismic traverses, which are of ~2,000 km in total length and across all five magnetic zones. Integration of magnetic and seismic data enables us to gain a better 3D mapping on the basin structures. It is shown that the transition from the southwest sub-basin to the east sub-basin is characterized by a major ridge formed probably along a pre-existing fracture zone, and by a group of primarily west-dipping faults forming an exact magnetic boundary between zones D and E. The northwest sub-basin has the deepest basement among the three main sub-basins (i.e., the northwest sub-basin, the southwest sub-basin, and the east sub-basin). Our seismic data also reveal a strongly faulted continent–ocean transition zone of about 100 km wide, which may become wider and dominated with magmatism or transit to an oceanic crust further to the northeast.

Keywords South China Sea · Magnetic anomaly · Seismic reflection · 3D analytic signal · Magnetic depth · Continent–ocean transition zone

C.-F. Li (✉) · Z. Zhou · B. Chen · J. Geng
State Laboratory of Marine Geology, Tongji University, 200092 Shanghai, China
e-mail: cfl@tongji.edu.cn

J. Li
2nd Institute of Oceanography, State Oceanic Administration, Hangzhou, 310012 Zhejiang, China

Introduction

The South China Sea basin evolved from Cenozoic continental margin rifting and subsequent seafloor spreading. It consists of three major sub-basins, namely, the east sub-basin, the northwest sub-basin, and the southwest sub-basin (Fig. 1). Despite extensive geological studies, the opening mechanism of the South China Sea still remains as an enigma. In addition, there have been continued debates on whether the present-day SCS basin experienced primarily a single episode or multiple episodes of extension and seafloor spreading and, if multiple, in what sequence the three sub-basins evolved (e.g., Taylor and Hayes 1980; Ru and Pigott 1986; Briais et al. 1993; Yao et al. 1994; Li et al. 2007b).

These debates seem to be unsolvable before a dedicated deep sea drilling project to be carried out in the South China Sea ocean basin. The water depths of the deep ocean basin range from about 3.5 to 4.5 km, and the sediments

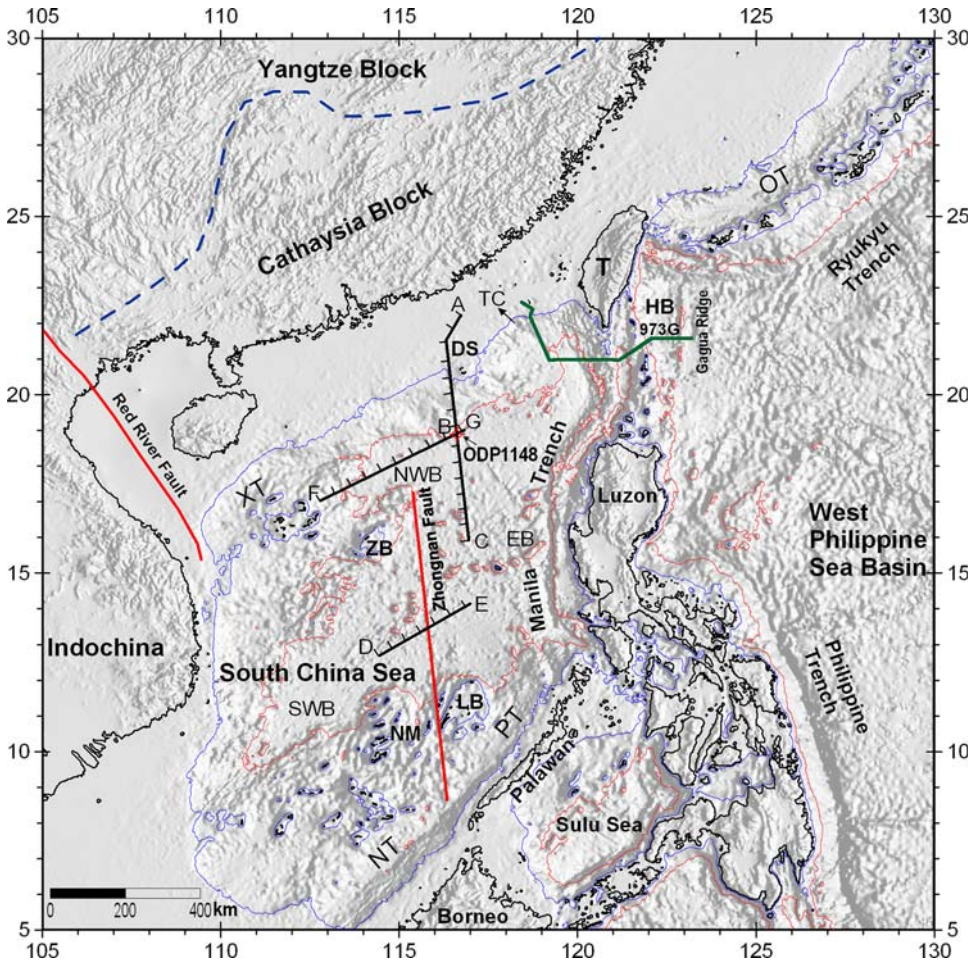

Fig. 1 Shaded relief map showing major tectonic regimes in the South China Sea region. AB BC FG, DE, and 973G are seismic sections. Two isobaths shown on the map are 500 and 3,000 m, respectively. *NT* Nansha trough; *DS* Dongsha rise; *HB* Huatung basin; *EB* east sub-basin; *SWB* southwest sub-basin; *NWB* northwest sub-basin; *OT* Okinawa trough; *PT* Palawan trough; *T* Taiwan island; *TC* Taiwan canyon; *XT* Xisha trough; *ZB* Zhongsha (Macclesfield) bank; *LB* Liyue (Reed) bank; *NM* Nansha Massif (Dangerous Grounds)

are mostly <2 km in thickness. The South China Sea basin is therefore a feasible target for future deep sea drilling and coring activities. But before these are actually implemented, geophysical investigations and data processing and interpretation remain to be perhaps the best means to study regional geodynamics. Furthermore, careful geophysical data analyses will lead to solid characterizations of future potential drilling sites.

The South China Sea is located at the junction of the Eurasian plate, the western Pacific plate, and the Indo–Australian plate (Fig. 1). Besides this unique geological setting, several other attributes make it an ideal natural laboratory for studying continental break-up and basin formation. Its relatively small size facilitates easy tectonic comparisons between the two conjugate continental margins. Meanwhile, the South China Sea is among the largest of the western Pacific marginal seas and is well suited for studying various plate boundary activities, such as continental margin rifting (e.g., Hayes and Nissen 2005), seafloor subduction (the Manila Trench; e.g., Li et al. 2007a), strike slip faulting (the Red River fault; e.g., Clift and Sun 2006), as well as active orogenic processes (Taiwan; e.g., Hsu and Sibuet 1995; Huang et al. 2001) (Figs. 1, 2).

In this paper, we focus our study on the internal structures of the South China Sea basin and its adjacent northern continental margin (Fig. 2), using magnetic and deep reflection seismic data. This work shows various magnetic differences within the deep sea basin, through a rigorous flow of magnetic data processing. We also base our work on newly obtained deep reflection seismic lines passing through all five magnetic zones in the area (Fig. 1).

Geophysical data

The total field magnetic data (Fig. 3) are compiled by Geological Survey of Japan and Coordinating Committee for Coastal and Offshore Geoscience Programmes in East and Southeast Asia (CCOP) (1996). The original data are from a variety of different sources, with different time, scales, and grid spacings. Our working area is from 110°E to 124°E in longitudes and 8°N to 25°N in latitudes. We interpolate the data into a 998 × 1,226 grid using the

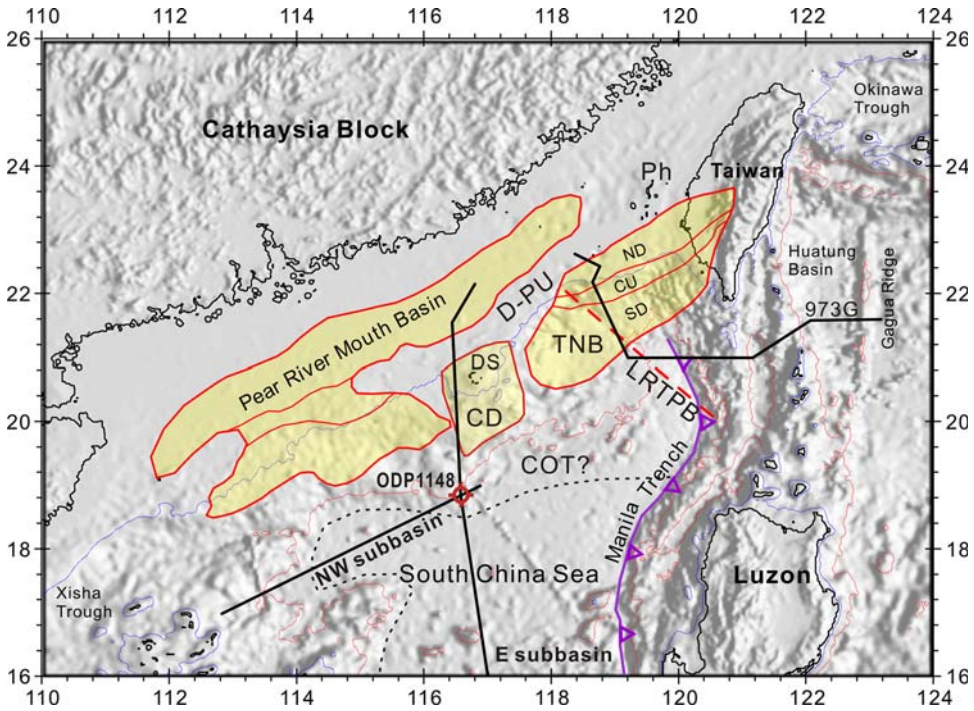

Fig. 2 Shaded relief map showing major Mesozoic and Cenozoic tectonic units. Two isobaths shown on the map are 500 and 3,000 m, respectively. *CD* Chaoshan depression; *COT* continent–ocean transition zone; *DS* Dongsha rise; *D-PU* Dongsha-Penghu uplift; *Ph* Penghu; *LRTPB* Luzon-Ryukyu transform plate boundary; *TNB* Tainan basin; *ND* Northern depression; *CU* Central uplift; *SD* Southern depression

minimum curvature algorithm (Briggs 1974), and the bin size is fixed at 1.55 × 1.55 km^2. Data processing includes upward continuation, power spectrum analysis, analytic signal analysis, and reduction to the pole. All these procedures are aimed at gaining in-depth understandings on distributions and magnetizations of magnetic sources and their regional variations.

Table 1 lists acquisition parameters of deep reflection seismic lines shown in Fig. 1. Line BC passes through the northwest sub-basin and part of the east sub-basin, line DE extends from the southwest sub-basin to the east sub-basin, line FG extends across the northwest sub-basin, and line 973G traverses the northeastern corner of the South China Sea. As can be seen from Fig. 1, these seismic lines pass through all five magnetic zones in the area, and hence allow easy correlations of deep crustal structures between different geological zones. All seismic data are in standard SEGY format and are loaded onto a SUN workstation for interactive interpretation.

Magnetic zoning

Total field magnetic anomaly

We first study total field magnetic anomalies (Fig. 3) of the South China Sea basin, which roughly corresponds to the area with water depths larger than 3,000 m. Magnetic anomalies suggest that the South China Sea basin can be divided into five magnetic zones. Zone A is approximately a triangular area confined by the offshore south China magnetic anomaly (SCMA), the Taiwan Orogen, the Luzon Arc, and the Luzon-Ryukyu Transform Plate Boundary (LRTPB) (Hsu et al. 1998, 2004; Sibuet et al. 2002; Li et al. 2007b). East-west striking, small wavelength, magnetic anomalies, recognized by Hsu et al. (1998) and Sibuet et al. (2002), are clearly visible in zone A.

Zone B and zone A are separated by the LRTPB (Fig. 2), across which significant contrasts in magnetic and seismic patterns have been identified (Hsu et al. 1998; Sibuet et al. 2002; Li et al. 2007b). Zone B is approximately a circular feature showing no clear magnetic lineation. Massive volcanic intrusions and extrusions are found on numerous multi-channel reflection seismic sections passing through zone B (Sibuet et al. 2002; Tsai et al. 2004; Wang et al. 2006; Li et al. 2007b). Hsu et al. (2004) suggested that this area could also belong to an oceanic domain.

Zone C is to the southwest of zone B and is limited within the northwest sub-basin. It is bounded to the south by a noticeable negative magnetic anomaly (M1 in Fig. 3). East-west striking anomalies within zone C are clearly identifiable, but they appear to have weaker contrasts and longer transverse wavelengths compared to those in zone D.

Magnetic zone D corresponds to the east sub-basin and is bounded to the north by M1 and to the south by another distinct negative magnetic anomaly that is similar to M1 (M2 in Fig. 3). M1 and M2 are nearly symmetric with respect to the relict spreading center, where a chain of

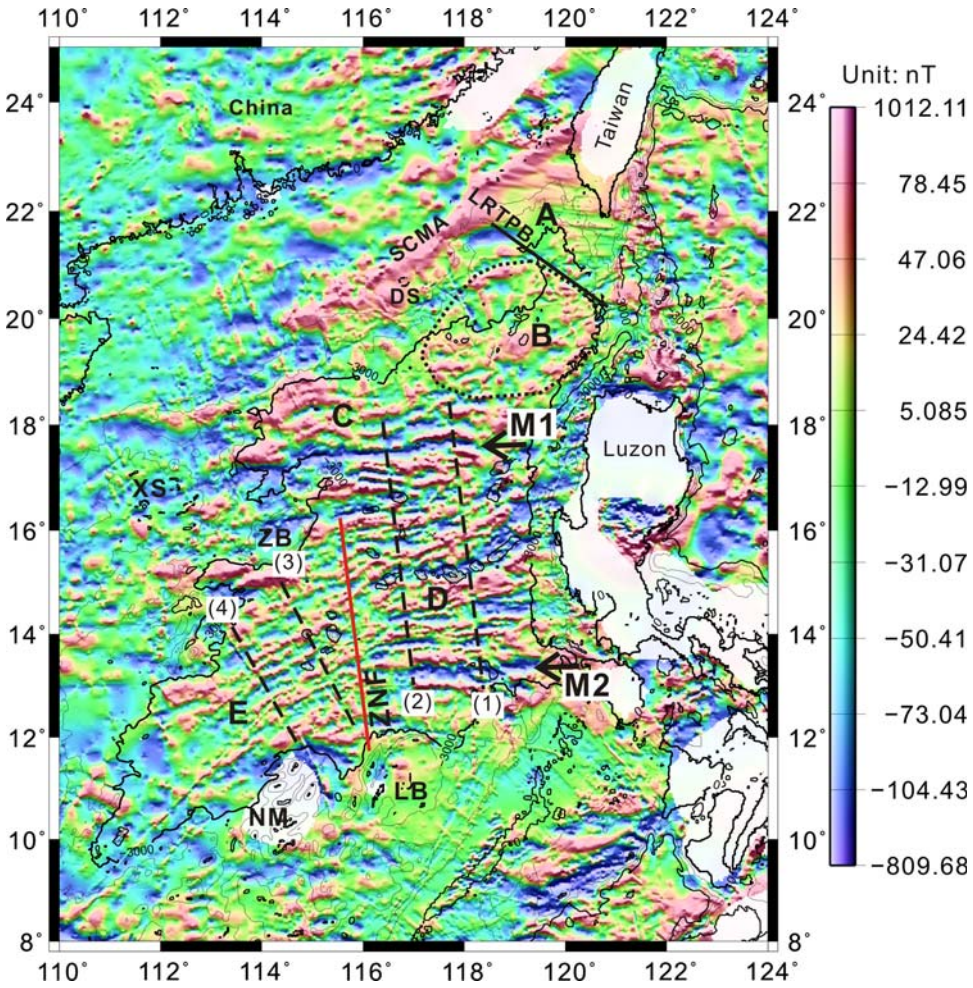

Fig. 3 Map of total field magnetic anomalies. This map shows five major magnetic zones (*A*, *B*, *C*, *D*, and *E*). *M1* and *M2* are two major magnetic anomaly bounding the zone *D*. *Dashed lines 1*, *2*, *3*, and *4* are four magnetic traverses from which magnetic data are to be extracted (Fig. 4) and their power spectra are to be calculated (Fig. 5). *ZNF* Zhongnan fault; *LRTPB* Luzon-Ryukyu transform plate boundary; *DS* Dongsha rise; *SCMA* offshore south China magnetic anomaly; *XS* Xisha; *ZB* Zhongsha (Macclesfield) Bank; *LB* Liyue (Reed) bank; *NM* Nansha Massif (Dangerous Grounds). The *dashed circle* outlines the zone *B*

Table 1 Acquisition parameters for seismic lines used in this study

Line names	973G	Lines AB, BC, DE, FG
Acquired by	GMGS[a]	SCSIO[b]
Acquisition date	2001	2001
Streamer channel	240	48
Record length (s)	10.024	12.0
Sampling rate (ms)	2	2
Receiver interval (m)	12.5	25.0
Shot interval (m)	50	50
Airgun volume (in.^{3})	3,000	1,370 or 1,520

[a] *GMGS* Guangzhou Marine Geological Survey, Chinese ministry of land and resources

[b] *SCSIO* South China Sea Institute of Oceanology, Chinese Academy of Sciences

volcanic seamount developed after the cession of spreading at about 16 Ma (Taylor and Hayes 1980, 1983; Jin et al. 1989; Pautot et al. 1986; Briais et al. 1993; Hsu et al. 2004; Yan et al. 2006). Magnetic anomalies in zone D have large amplitudes and align in a roughly east-west orientation.

The magnetic patterns in the southwest sub-basin (magnetic zone E) differ significantly from those in zone D, not only in amplitude, but also in orientation. Zone E and zone D are sharply divided by the Zhongnan fault (Figs. 1, 3), which is a transform boundary between the southwest sub-basin and the east sub-basin (Yao 1995; Jin et al. 2002; Li et al. 2007b).

Power spectrum analyses

Although the contrast in magnetic amplitudes and orientations is clear between zone D (east sub-basin) and zone E (southwest sub-basin), we are yet unsure if there are any magnetic frequency differences between the two zones. Power spectra of magnetic data can be valuable sources of information in studying magnetic depths and layering. For this purpose, we extract four transactions (Figs. 3, 4) from the magnetic grid and study their log power spectra using fast Fourier transform (Fig. 5). Transactions (1) and (2) are in the east sub-basin and (3) and (4) in the southwest sub-basin, and they are all nearly perpendicular to the magnetic strikes.

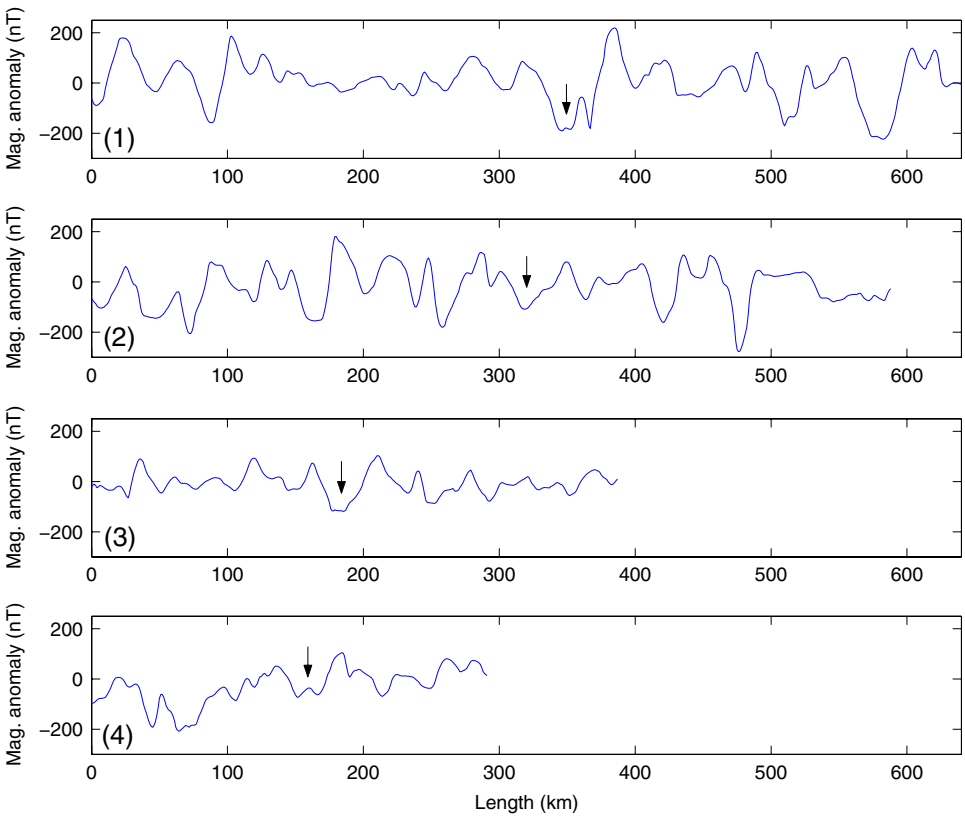

Fig. 4 Four magnetic profiles from the South China Sea ocean basin. See Fig. 3 for locations. The downward pointing arrows indicate the points of the relict spreading center of the South China Sea

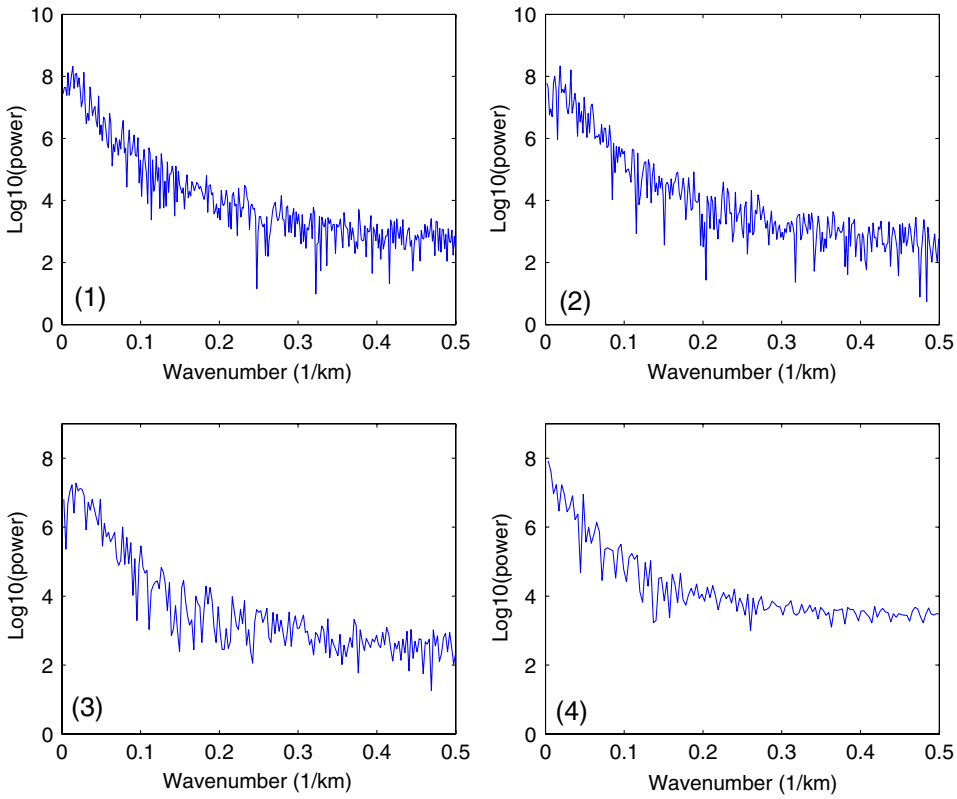

Fig. 5 Log power spectra of the four magnetic profiles in Fig. 4

From the total field magnetic map (Fig. 3), we can see larger magnetic amplitudes in the east sub-basin than in the southwest sub-basin. However, as evidenced by Fig. 5, there are no big differences in power spectra, except that the spectrum of transaction (4) deviates a little bit from others at medium to high wavenumbers and shows more short-wavelength components. This implies no significant differences in magnetic depth distributions between the two sub-basins, despite their apparent differences in magnetic amplitudes. The amplitude contrast is due more likely to different mineral contents and thereby different magnetizations in basement rocks. It is also possible that slightly higher heat flows in the southwest sub-basin (see e.g., Taylor and Hayes 1983) may result in a thinner magnetized layer leading to weaker magnetic anomalies of smaller wavelengths. Magnetic contrast between the east and the southwest sub-basins may also suggest differences in their spreading rates, as the anomalous skewness of magnetic anomalies can be dependent on spreading rates (Dyment and Arkani-Hamed 1992).

Upward continuation

The original total field magnetic data contain noises from various sources. In particular, track footprints can be easily noticed west of the Dongsha Islands on Fig. 3. Noises and shallow magnetic sources could disguise deep or regional structures. Upward continuation is a smoothing process that can suppress noise, and tends to accentuate anomalies caused by deep sources at the expense of anomalies caused by shallow sources (Blakely 1996). As an initial effort in suppressing noises, we upward continue the original magnetic data (Fig. 3) by 5 km and the result is shown in Fig. 6. It can be instantly noticed by comparing Figs. 3 and 6 that most of the high-frequency noises are effectively suppressed and true magnetic patterns are enhanced. This new data set (Fig. 6) is used later in calculating 3D analytic signals and estimating depths to top bounds of magnetic sources.

Figure 7 shows the result of upward continuation of the original total field magnetic data in Fig. 3 by 20 km.

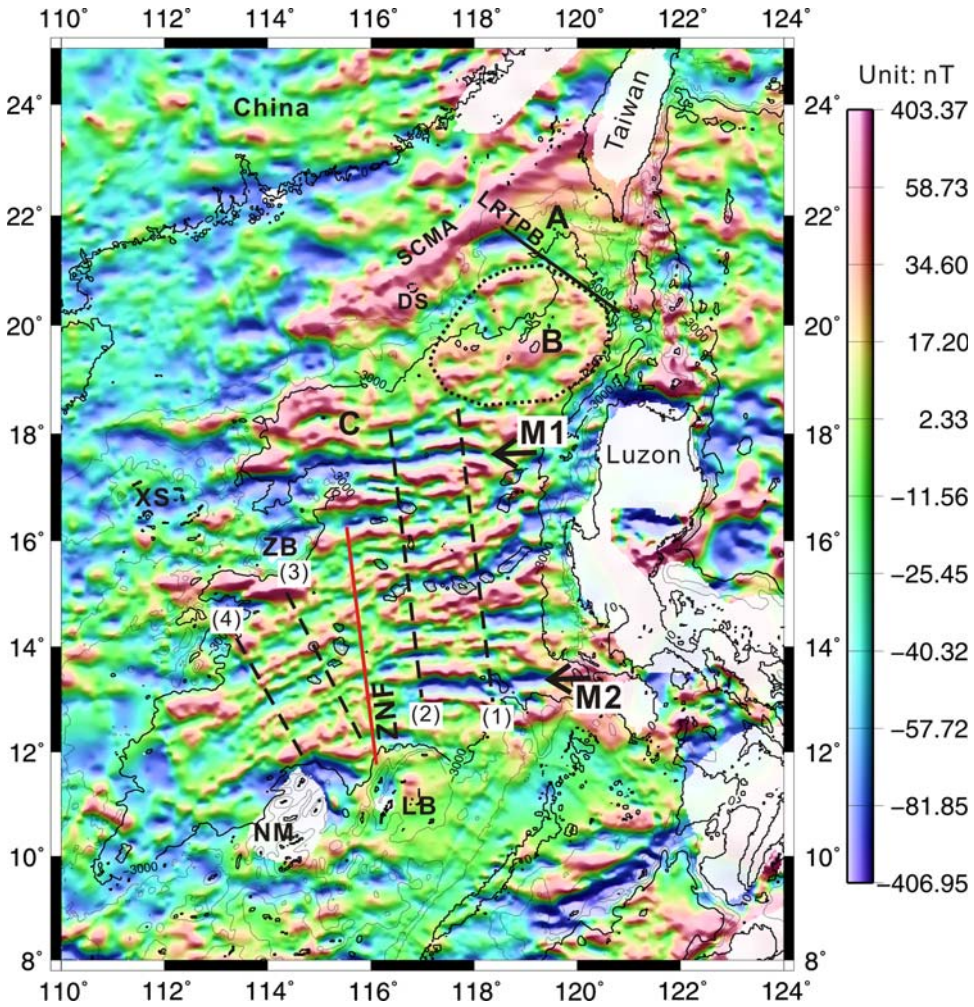

Fig. 6 Map of total field magnetic anomalies that is upward continued by 5 km in order to remove high-frequency noises. See Fig. 3 for notations

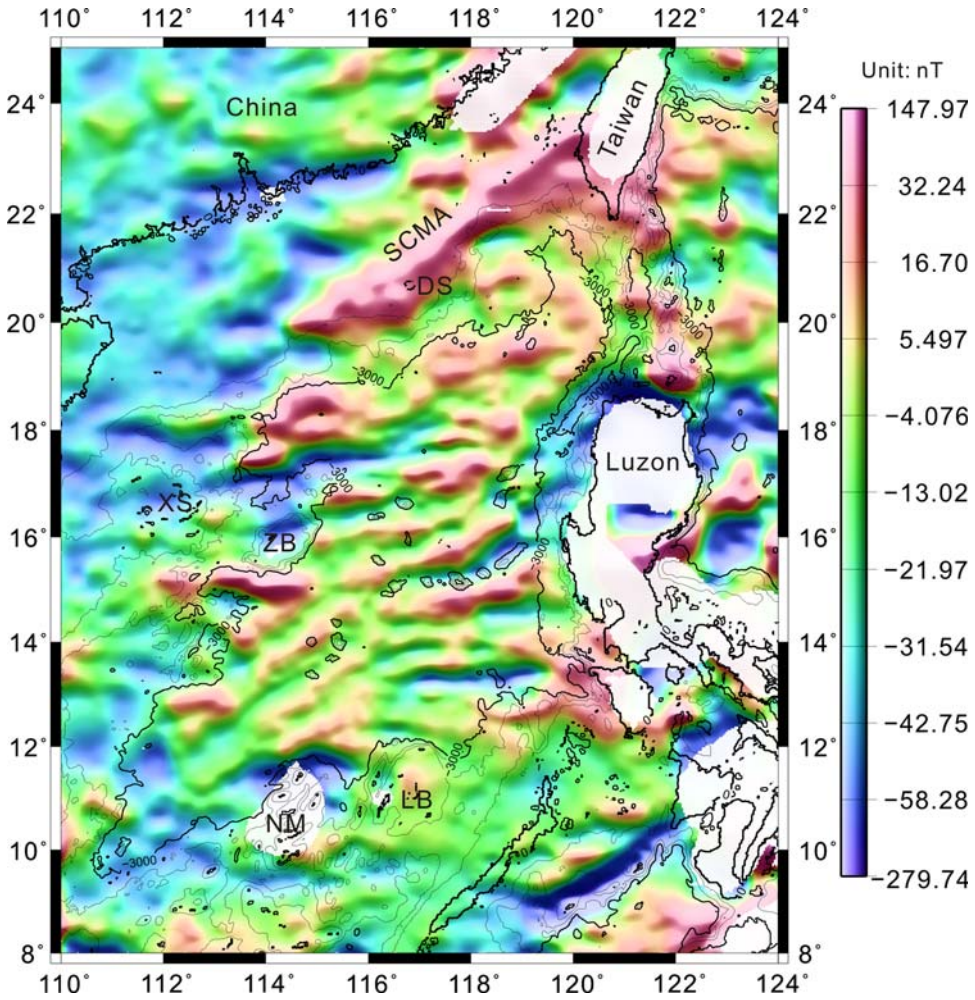

Fig. 7 Map of upward continuation of the total field magnetic data by 20 km. *SCMA* offshore south China magnetic anomaly; *DS* Dongsha rise; *XS* Xisha; *ZB* Zhongsha (Macclesfield) bank; *LB* Liyue (Reed) bank; *NM* Nansha Massif (Dangerous grounds)

Although the changes after the upward continuation are significant, the five magnetic zones and their boundaries can still be readily recognized. In zone A, east-west striking magnetic anomalies largely disappear, indicating that the magnetic sources of these anomalies are of relatively shallow depths. The relict transform fault LRTPB between zone A and B is now characterized by a magnetic low. The circular feature of zone B is still recognizable. While original linear magnetic anomalies in Zone C become less obvious, both zone D and E still show clear magnetic lineations. The Zhongnan fault between zone D and E is also clearly identified after upward continuation, suggesting it to be a deep crustal fault. The relict spreading centers in both the southwest and the east sub-basins are characterized by magnetic lows, and there is a big horizontal offset between the two spreading centers across the Zhongnan fault (Fig. 7). This offset and contacting relationship is not so clear on the original magnetic map (Fig. 3). One can also note that the SCMA becomes a more outstanding feature on the map upward continued by 20 km, indicating that the magnetic sources inducing the SCMA are deeply rooted.

3D analytical signal amplitudes

The South China Sea basin is located at low latitudes where small inclination angles can severely skew magnetic anomalies and bias our interpretation. In addition, shallow magnetic sources from seafloor spreading have alternate remnant polarizations due to the magnetic reversal. These two facts render it difficult to perform reduction to the pole for magnetic data from the deep basin of the South China Sea. However, we are still extremely interested in knowing the exact positions and characters of magnetic boundaries as this information is vital for better understanding of regional geodynamics.

To circumvent the afore-mentioned problems, we resort to the 3D analytic signal, which can be defined as (Nabighian 1984; Ofoegbu and Mohan 1990; Roest et al. 1992)

$$A(x,y) = (\partial \mathrm{M}/\partial x)\vec{\mathrm{x}} + (\partial \mathrm{M}/\partial y)\vec{\mathrm{y}} + i(\partial \mathrm{M}/\partial z)\vec{\mathrm{z}}, \qquad (1)$$

where M is the magnetic field anomaly, and $\vec{\mathrm{x}}, \vec{y}, \vec{z}$ are unit vectors in x, y and z directions, respectively. The 3D analytic signal amplitude can be defined by a vector addition of the two real components in horizontal directions and the

imaginary component in vertical direction (Roest et al. 1992), i.e.,

$$|A(x,y)| = \sqrt{(\partial \mathrm{M}/\partial x)^2 + (\partial \mathrm{M}/\partial y)^2 + (\partial \mathrm{M}/\partial z)^2}. \qquad (2)$$

Later, Hsu et al. (1996) generalized the definition of analytic signal amplitude to achieve high resolutions by incorporating higher order derivatives. Alternatively, Ofoegbu and Mohan (1990) used a scalar addition for the two horizontal derivatives, but Mohan and Anand Babu (1995) proved that 3D analytic signal based on the scalar addition are identical to that based on the vector addition. In essence, analytic signal amplitude is equivalent to the total gradient. For vertical contact models, which can be assumed for seafloor magnetizations such as within the South China Sea basin, 3D analytic signal amplitude can be independent of inclinations and declinations of source magnetizations and the Earth's magnetic field, though for general cases this statement is not strictly valid (Agarwal and Shaw 1996; Salem et al. 2002; Li 2006). The particular low-latitude location and strong remnant magnetic lineation of the South China Sea Basin justify the use of analytic signal analysis, which can complement and/or replace the reduction to the pole. Analytic signal amplitudes can help with data interpretation, since for vertical contact models, such as for the magnetic sources from continental margin rifting and drifting in the South China Sea, the maximum analytic signal amplitudes are always directly above the magnetic contacts.

Since the analytical signal amplitude is a combination of the first-order derivatives of magnetic anomalies, it inevitably enhances random noise, gridding artifacts, and track corrugations. Track footprints are easily observed from the original total field magnetic map (Fig. 3). To avoid these problems, we first upward continue the total field magnetic data by 5 km (Fig. 6), and then calculate the analytic signal amplitude.

The analytic signal amplitudes show a big contrast between the east and the southwest sub-basins (Fig. 8), roughly along the Zhongnan fault. The high analytic signal amplitudes of the east sub-basin suggest that the magnetic sources there are of higher magnetizations and sharper contrasts. This is consistent with observations from the total field magnetic map (Fig. 3) and with early deductions

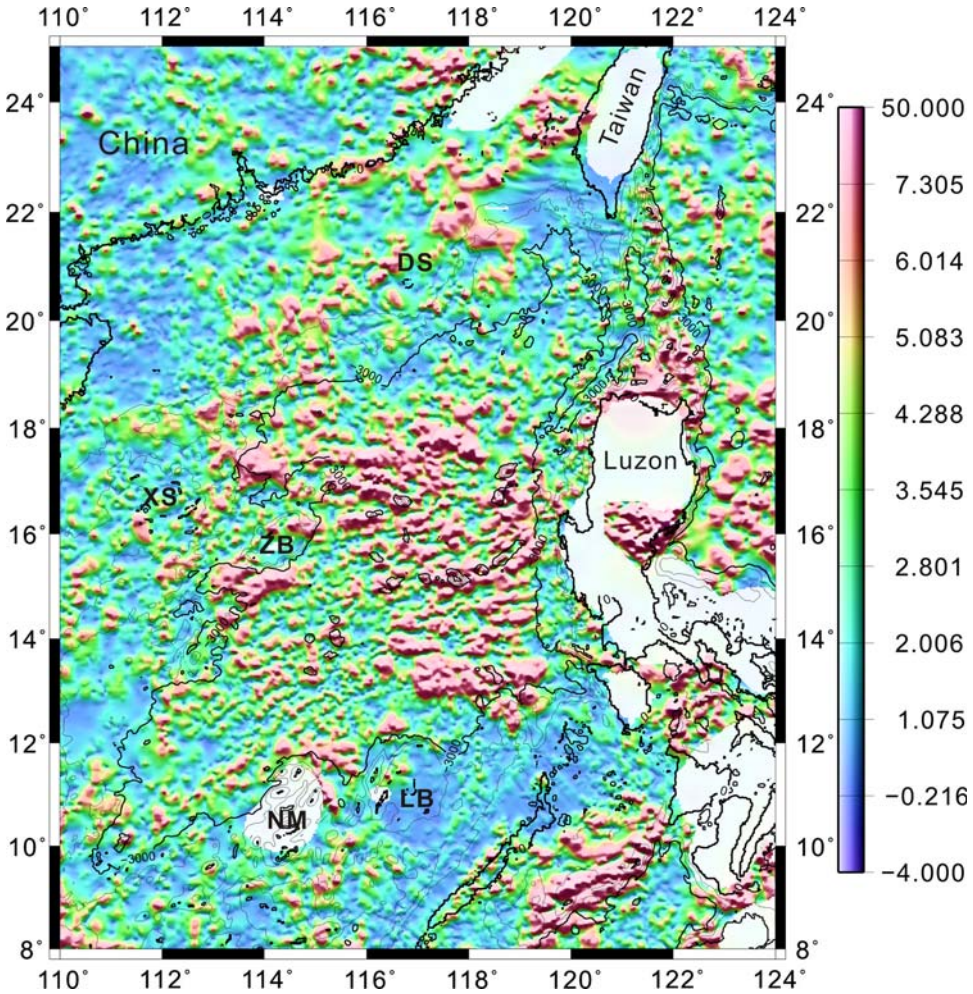

Fig. 8 Map of the 3D analytical signal amplitudes. *DS* Dongsha rise; *XS* Xisha; *ZB* Zhongsha (Macclesfield) bank; *LB* Liyue (Reed) bank; *NM* Nansha Massif (Dangerous grounds)

from power spectrum analyses. The highest analytic signal amplitudes show up along the northern and southern edges and the relict spreading center of the east sub-basin. The northwest sub-basin (magnetic zone C) shows analytic signal amplitudes lower than that of the east sub-basin but close to that in the southwest sub-basin. Magnetic zone B becomes less characteristic and has small values on the map of analytic signal amplitudes (Fig. 8), indicating relatively uniform distributions and weak magnetizations of magnetic sources within this circular feature. Just like on the total magnetic field map (Fig. 3), magnetic zone A again appears as a unique area with very small analytic signal amplitudes, and it is also clear that the relict transform boundary LRTPB serves as the southern boundary of magnetic zone A.

Another important observation is that the analytic signal amplitudes reveal the northern margin of the Tainan basin (Fig. 2), which is a Cenozoic rifting basin (Lee et al. 1993; Tzeng 1994; Lin et al. 2003) but with possibly thick Mesozoic sediments underneath (Li et al. 2007b, 2008). On the total field magnetic map (Fig. 3), the northern margin of the Tainan basin (Fig. 2) is rather vague and the basin itself does not correlate with a unique magnetic pattern. However, on the map of the analytic signal amplitudes, there is a distinct magnetic boundary corresponding exactly with the northern margin of the Tainan basin and the basin shows itself as a magnetically uniform area, contrasting sharply to the Dongsha-Penghu uplift to the north. In addition, the area corresponding to the Chaoshan depression, which is a Mesozoic sedimentary basin (Li et al. 2008), also has low and uniformly distributed analytic signal amplitudes, indicating it has sparse and weak magnetic distribution. These findings are supported by reflection seismic data that show thick Mesozoic sediments within the Chaoshan depression (Li et al. 2008).

The SCMA as a prominent feature on the total field magnetic map (Fig. 3) becomes narrower and less continuous on the map of the analytic signal amplitudes. Based on these observations and the fact that analytic signal amplitudes highlight magnetic contrasts, we interpret that the SCMA may represent a zone of contrast between two magnetic domains. This interpretation is consistent to results from Euler deconvolution and reduction to the pole (Li et al. 2008).

Reduction to the North Pole

For comparison, we show the magnetic data reduced to the pole for the northeasternmost continental margin of the South China Sea basin (Fig. 9). Reduction to the pole theoretically works on magnetic data in a way similar to analytic signal analysis, despite different assumptions and technical details inherent in these two transformations (Roest et al. 1992; Blakely 1996; Li 2006).

Similar to the analytic signal amplitudes, total field magnetic data reduced to the pole also clearly reveal a sharp northern boundary of the Tainan basin. The SCMA also becomes less continuous and less prominent after the reduction. Magnetic anomalies after the reduction to the pole are also weak in the proximity of the Chaoshan depression. Therefore, magnetic data reduced to the pole and the analytic signal amplitudes can cross-check each

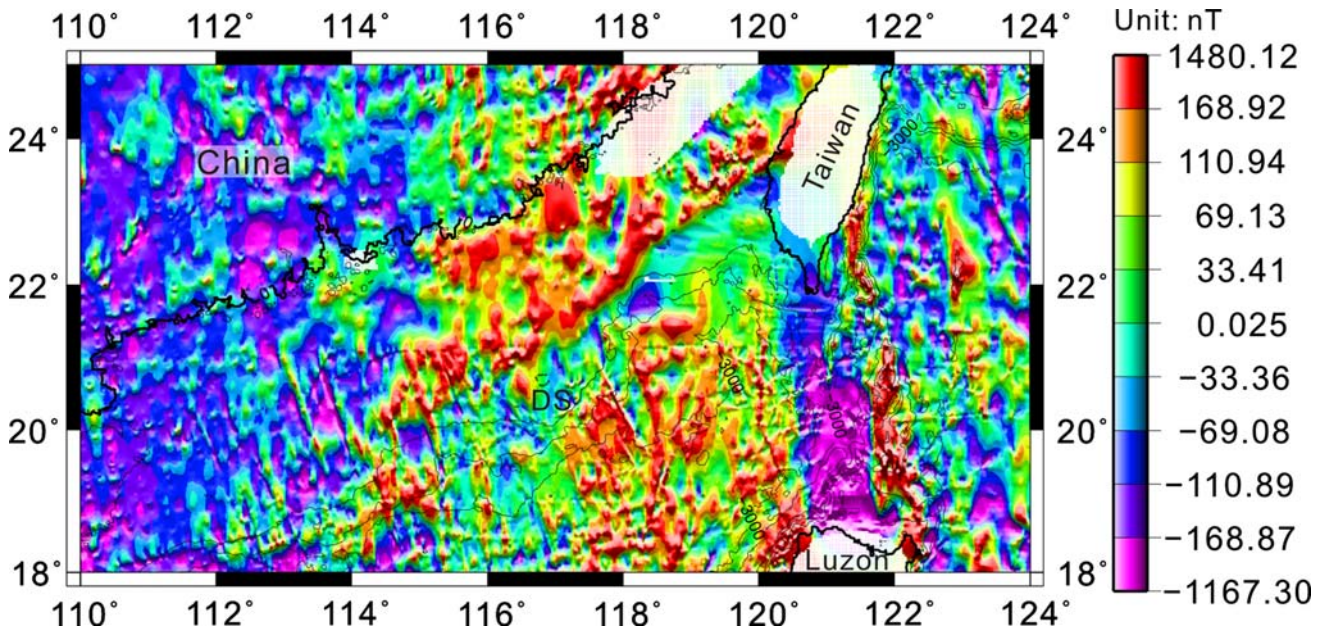

Fig. 9 Map of the magnetic data reduced to the North Pole. *DS* Dongsha rise

other, and both suggest weak magnetizations of the Chaoshan-Tainan depositional system (Li et al. 2008).

Although reduction to the pole at low latitudes would produce short-wavelength artifacts elongated in the direction of the declination (Blakely 1996), we can still observe a sharp contrast between magnetic zone A and B (Fig. 9). The circular feature of zone B seems to be more evident than on the total field map. Again, magnetic zone A shows very weak magnetization.

Magnetic locations and depths

Roest et al. (1992) developed a practical method to estimate the positions and depths of magnetic contrasts from the analytic signal amplitudes. Within each data window, they first applied the method of Blakely and Simpson (1986) to automatically detect the maxima in analytic signal amplitudes. With these maxima they attempted to determine the linear strikes of the maxima, and then estimate the depths to the tops of magnetic sources using the half widths of fitted bell-shaped functions over the cross sections of linear trends of the analytic signal amplitude maxima (Nabighian 1972, 1974; Atchuta Rao et al. 1981).

In this study we use the computer program ASDEP of Phillips (1997) to estimate the magnetic depths. This program is similar in practice to the method of Roest et al. (1992). Figure 10 plots the locations of magnetic contrasts and estimated depths. It is obvious from Fig. 10 that the South China Sea basin has the shallowest magnetic sources on the map, mostly equal to or <5 km below sea level. Magnetic sources within the West Philippine Sea Basin or on the northern South China Sea continental margin are appreciably deeper. Despite the apparent contrast in analytic signal amplitudes between the southwest and the east

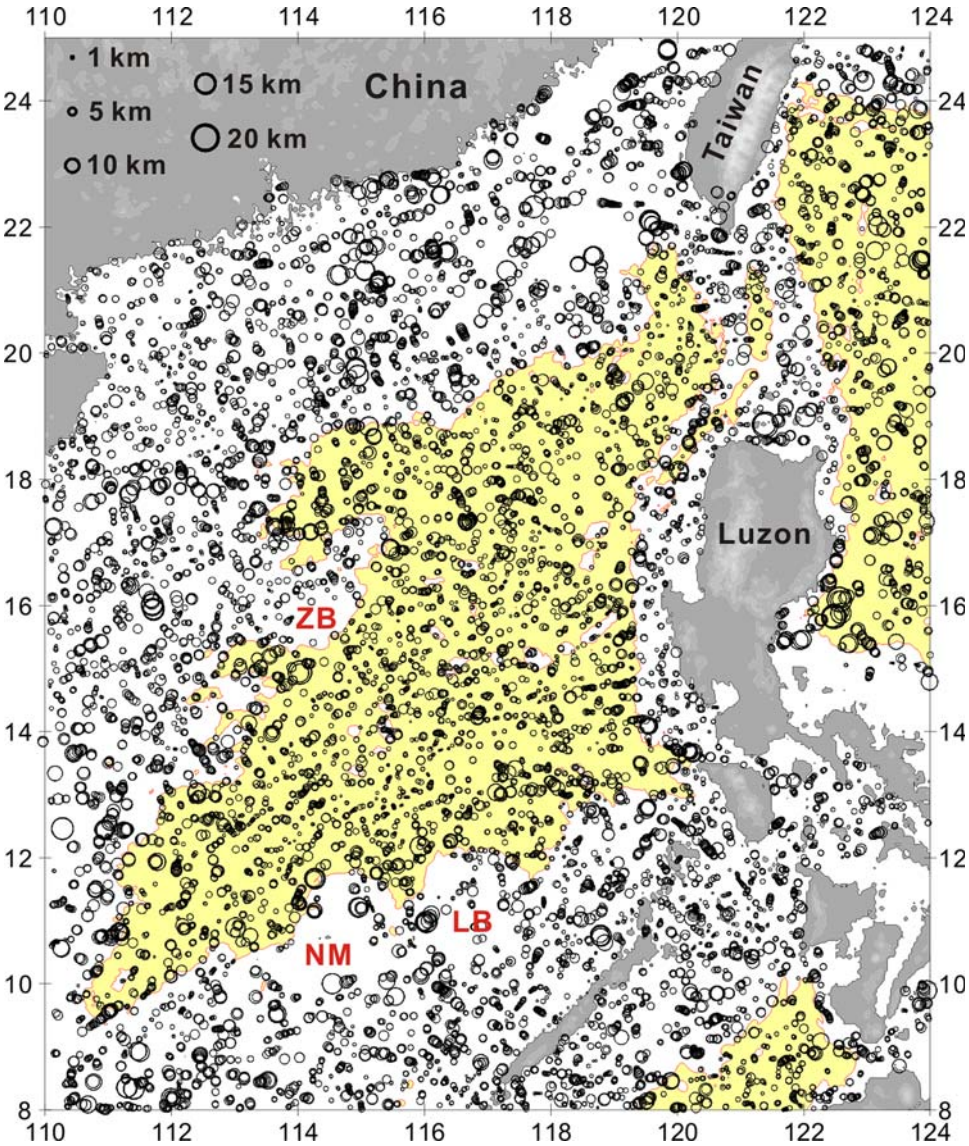

Fig. 10 Estimated depths and locations of magnetic sources in the South China Sea area. Areas with water depths larger than 3,000 m are marked by *yellow backgrounds*. *ZB* Zhongsha (Macclesfield) bank; *LB* Liyue (Reed) bank; *NM* Nansha Massif (Dangerous grounds)

sub-basins, there appears to be no differences in depths to the tops of magnetic sources. This result is consistent to our early deductions based on power spectrum analyses, and can be further verified in the next section by reflection seismic data. Therefore, the differences in total field magnetic strengths and analytic signal amplitudes between the southwest and the east sub-basins are more likely due to slightly different magnetizations and mineral compositions of the oceanic crust. It is possible that shallow magmatic materials in the southwest sub-basin are more silicic than those in the east sub-basin. This interpretation supports two distinct crustal settings across the Zhongnan fault, and is in line with the statement of Pautot et al. (1986) that the oceanic crust of the west sub-basin was perhaps emplaced within stretched continental crust whereas the crust of the east sub-basin formed in an area already floored by an oceanic crust. This pre-existing oceanic crust might be the crust of the northwest sub-basin, which formed earlier than the east sub-basin.

Li et al. (2008) also studied the magnetic depths of the northeastern South China Sea continental margin using Euler deconvolution, and found that magnetic sources inducing the SCMA are mostly within the upper crust, with depths from a few kilometers to about 20 km. The magnetic depths around the SCMA estimated from analytic signal amplitudes are consistent with those estimated from Euler deconvolution of the total field magnetic anomalies.

Seismic structure

Although extensive reflection seismic studies have been carried out in the area, most data are presented sporadically and thus incapable of offering an overall view on the basin structures. Here we made systematic studies on a new set of deep reflection seismic data of a total length of about 2,000 km (Fig. 1). These seismic lines pass through all major zones within the South China Sea basin, allowing us to examine their crustal structures and tectonic differences in cross-sectional views. Combining magnetic and seismic data together allows us to effectively study the 3D structures of the basin.

Northwest and east sub-basins

Seismic line ABC goes from the continental margin to the deep basin (Figs. 1, 10). The continental slope, approximately from the Dongsha Islands to a listric fault on seismic line ABC (Fig. 11), is dominated by faults, many of which reach the seafloor. The listric fault bounds a big

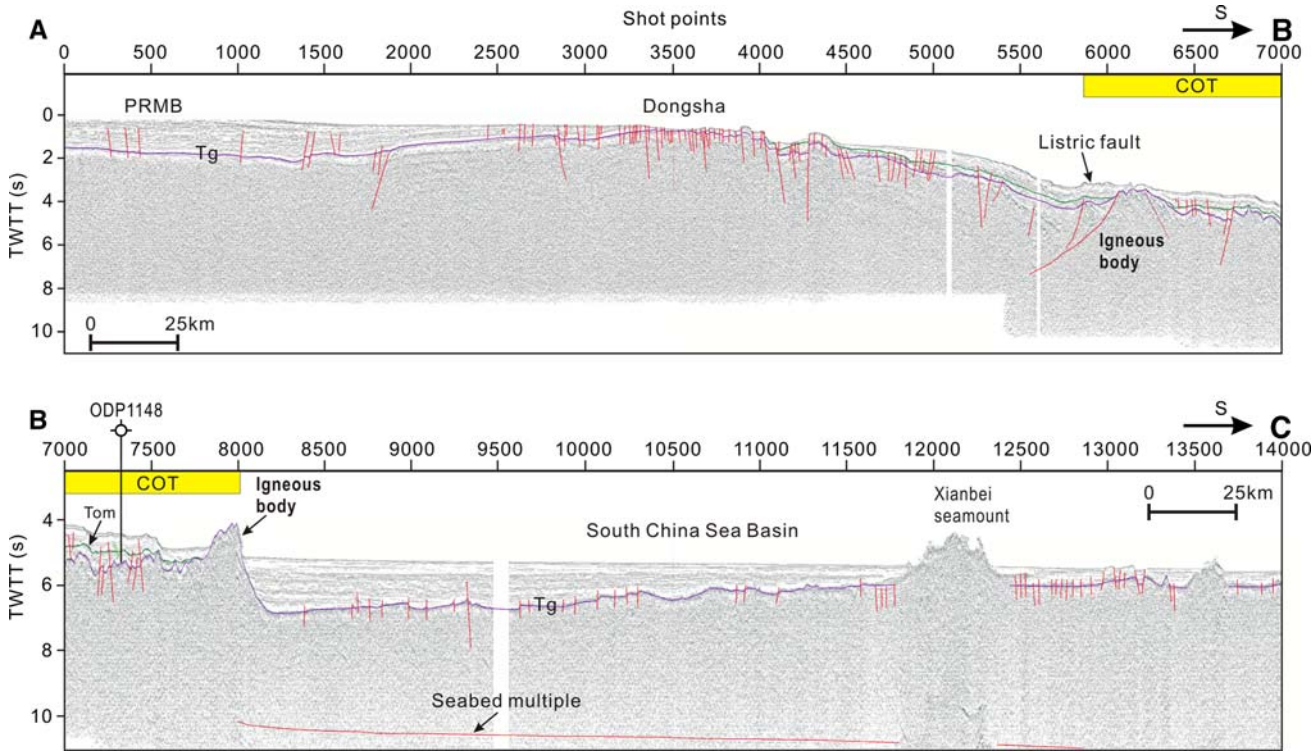

Fig. 11 Seismic sections AB and BC showing the structures in the northern South China Sea continental margin, the continent–ocean transition zone (*COT*), and the deep see basin. Tg is the Cenozoic basement. Horizon Tom represents the unconformity between the Oligocene and the Miocene

igneous body to its south, and a half-graben to its north. The listric fault and associated graben are important features along the northern South China Sea continental margin, and may be related to high heat flow (Shi et al. 2003). From the listric fault southward to a second major igneous body around shot point 8000 is the densely faulted continent–ocean transition zone (COT) (Fig. 11).

Line ABC is designed to pass through the Ocean Drilling Program (ODP) Site 1148 (Wang et al. 2000). The two interpreted horizons, Tom and Tg in Fig. 11, represent the Oilocene-Miocene boundary and the basement, respectively. From well-logging P-wave velocities obtained at ODP1148 (Fig. 12a), we build a time-depth curve at this location (Fig. 12b), which can be well approximated by a quadratic polynomial

$$d = 0.0003t^2 + 0.7155t - 2.4959, \quad (3)$$

where t stands for the two way travel time (in microseconds) and d is the depth (in meters) beneath the seafloor. This time–depth relationships will be used in estimating sediment thicknesses in the South China Sea basin. Cenozoic stratigraphy at ODP1148 is well studied (Wang et al. 2000; Li et al. 2004). However, along the northern margin of the South China Sea basin, the almost ubiquitous igneous bodies (e.g., around shot point 8000 in Fig. 11) separate the Cenozoic strata on the continent–ocean transition zone from those in the South China Sea basin. Therefore it is highly problematic to extrapolate the Cenozoic stratigraphy obtained at ODP1148 to the deep basin. The lack of detailed stratigraphic correlations within the South China Sea basin remains to be one of the major reasons why the Cenozoic opening history of the South China Sea remains controversial.

Thicknesses of Cenozoic strata in the deep basin decrease gradually from the northern edge southward to the relict spreading center (Fig. 11), an observation consistent with the cooling and subsidence model of oceanic lithosphere (Johnson and Carlson 1992; Turcotte and Schubert 2002). The average water depth of the deep basin is about 4,000 m, and the depth to the top of the oceanic crust (basin basement) ranges from about 4,400 to 5,900 m. High-angle faults in the basin basement are widespread (Fig. 11), most of which cut through only the uppermost part of the basement and lowermost section of the Cenozoic sediments. We interpret these faults to be associated with seafloor spreading of the South China Sea.

East and southwest sub-basins

Seismic line DE shows the transition zone between the east and southwest sub-basins (Fig. 13a). There are no apparent differences in sediment thicknesses and basement depths between the two sub-basins, but along line DE the water depth of the southwest sub-basin is slightly deeper than in the east sub-basin, by about 100 m. Early studies also suggested that the southwest sub-basin has deeper water

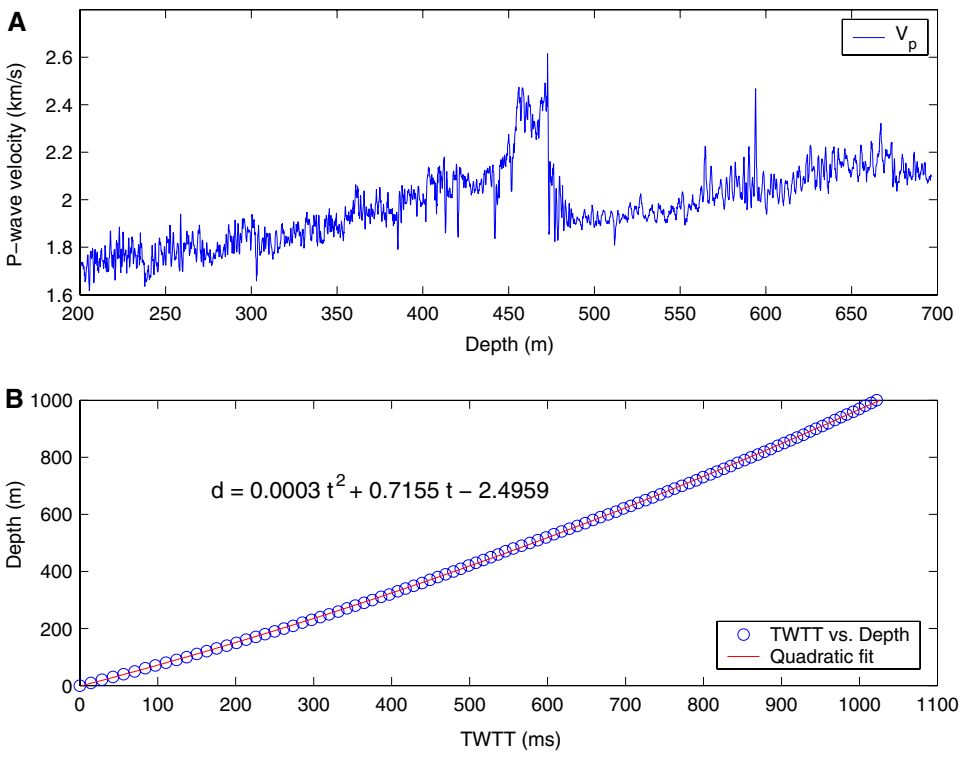

Fig. 12 **a** P-wave sonic logging velocity from the Ocean Drilling Program (*ODP*) site 1148. **b** calculated relationship between depth (m) versus two way travel time TWTT (ms)

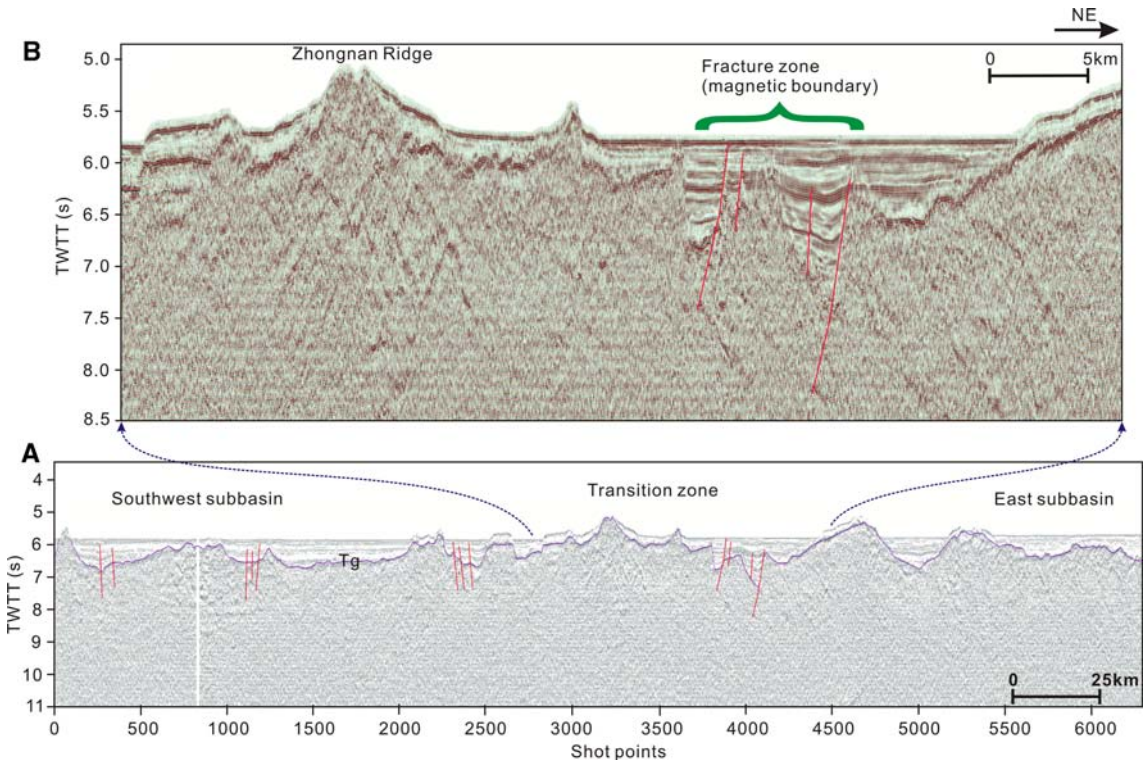

Fig. 13 **a** Seismic section DE showing the structures of the southwest sub-basin and the east sub-basin, as well as the transition zone in between. Tg is the Cenozoic basement. **b** The zoomed-in view on the transition zone structures

depth than the east sub-basin (Yao et al. 1994). The transition zone is composed of ridges (e.g., the Zhongnan Ridge) and a fracture zone (Fig. 13b). On the map view (Fig. 1), the Zhongnan Ridge is a north-south elongating structure between the east and southwest sub-basins. On the cross-sectional view, the ridge shows a V-shaped crest (Fig. 13b), which is similar to that of the Gagua Ridge in the west Philippine Sea basin (Fig. 1). Deschamps et al. (1998) argued that the Gagua ridge formed along an early fracture zone. Based on the bathymetrical structures and the chaotic seismic reflections of the Zhongnan ridge, it is possible that the Zhongnan ridge also formed along a pre-existing fracture zone between the two sub-basins.

To the east of the Zhongnan ridge, there developed a group of primarily west-dipping normal faults that bounds local grabens of abnormally thick sediments. What is more important is that this fault zone coincides with the magnetic boundary between the magnetic zone D and zone E.

Northwest sub-basin

Seismic line FG extends from the Xisha Islands northeastwards to the Dongsha area (Fig. 1). It passes through the northwest sub-basin and the ODP site 1148 (Fig. 14). Again, due to the presences of igneous bodies and boundary faults along the northern continental margin, stratigraphy revealed at ODP1148 cannot be easily extrapolated to the deep basin. The basement of the northwest sub-basin deepens slightly to the southwest, before it meets a major basement high (Fig. 14). To the west of the basement high is the heavily faulted continental margin and slope near the Xisha Islands. The northwest sub-basin has the largest thickness of Cenozoic sediments among all three sub-basins.

Discussions and conclusions

Regional magnetic data from the South China Sea basin reveal five distinct magnetic zones. The contrasts between these zones argue for a complicated opening mechanism and evolutionary history of the South China Sea, despite its relatively young age from about 37 or 32 to 16 Ma (Briais et al. 1993; Hsu et al. 2004). Magnetic zone A to the southwest of Taiwan Island appears to be sharply different from the three main sub-basins, namely the east, southwest, and northwest sub-basins, and it is likely that this zone may not be directly associated with the opening of the South China Sea. Indeed, Hsu et al. (1998, 2004) and Sibuet et al. (2002) argued that this area might be a trapped piece of the Philippine Sea Plate. Reflection seismic data (line 973G) passing through this zone show quite complicated

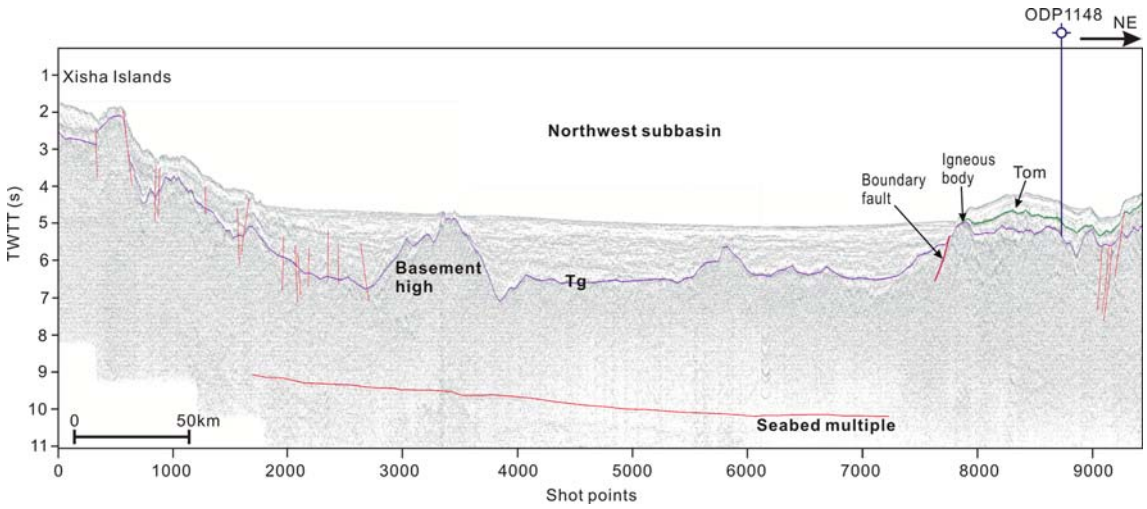

Fig. 14 Seismic section FG across the northwest sub-basin. Tg is the Cenozoic basement. Horizon Tom represents the unconformity between the Oligocene and the Miocene

structures, which may not be reasonably explained by a single oceanic or continental block (Li et al. 2007b).

Both the magnetic data reduced to the pole and the analytic signal amplitudes suggest that the offshore south China magnetic anomaly (SCMA) is not so continuous along its strike as it appears on the original total field magnetic anomaly map, and it represents a zone of magnetic contrast between the Dongsha-Penghu uplift and the Chaoshan-Tainan depositional system. Both magnetic data upward continued by 20 km and the analytic signal amplitudes support that the magnetic sources causing SCMA have large depths. Various reductions on the total field magnetic data also suggest very low magnetizations in the Chaoshan-Tainan depositional system. The east and the southwest sub-basins possess similar magnetic power spectra and depths to top bounds of magnetic sources, but they have obvious differences in the total magnetic field and analytic signal amplitudes. We attribute these magnetic contrasts to different tectonic settings where the two sub-basins were originally developed. The shallow crustal materials in the east sub-basin appear to be more mafic and thereby attain stronger remnant magnetization. We tend to agree with the argument of Pautot et al. (1986) that the oceanic crust of the west sub-basin was perhaps emplaced within a stretched continental crust whereas that of the east sub-basin formed in an area already floored by oceanic crust. However, we cannot exclude other possible contributors to the magnetic contrast between the east and the southwest sub-basins, such as differences in thicknesses of magnetized layers, spreading rates, and heat flows.

The transition zone between the east and southwest sub-basin is composed of ridges and faults. The Zhongnan ridge probably formed along a fracture zone, while to its east, a group of west-dipping faults characterize the magnetic boundary between the two sub-basins. The transition zone remains evident on the magnetic map with an upward continuation by 20 km, and the new map also shows a clear ridge jump from the east sub-basin to the southwest sub-basin. The transition from the northwest sub-basin to the east sub-basin is not so obvious on reflection seismic data, but is marked by a belt of large analytic signal amplitudes (Fig. 8) as well as by a strong negative magnetic anomaly (M1 on Fig. 3) on the total field magnetic map. Two other belts of high analytic signal amplitudes in the east sub-basin correspond with the relict spreading center and the southern margin of the east sub-basin, respectively.

Seismic line ABC reveals a broad continent–ocean transition zone (COT) of more than 100 km wide. This zone appears to be much wider or transits to an oceanic crust to the east (Hsu et al. 2004; Tsai et al. 2004; Wang et al. 2006). The continent–ocean transition is characterized by massive igneous intrusions and extrusions, dense faulting, strong basement deformation, localized high heat flow, and relatively quiet or uniform magnetization.

Crude magnetic depth estimation from analytic signal amplitudes indicates that the South China Sea Basin has statistically the shallowest distribution of magnetic sources in the area of study. This is consistent with the seafloor spreading model of the South China Sea, where the magnetic sources are located within the uppermost layer of the oceanic crust, at depths from about 4 to 6 km.

The opening history of the South China Sea is controversial due to the lack of accurate dating (Taylor and Hayes 1980; Pautot et al. 1986; Ru and Pigott 1986; Briais et al. 1993; Yao et al. 1994; Hsu et al. 2004; Hayes and Nissen 2005; Li et al. 2007b). There appears to be no significant differences in basement depths between the southwest sub-basin and the east sub-basin, but the water depths and heat

flows in the southwest sub-basin are slightly larger than in the east sub-basin. The northwest sub-basin apparently has the thickest Cenozoic sediments and deepest basement among all three sub-basins, and appears to be the oldest based on the simple depth-age relationship (Johnson and Carlson 1992; Turcotte and Schubert 2002). On the other hand, the northwest sub-basin seems to crosscut the presumably younger Zhongnan fault. To solve these problems and/or ambiguities, drilling and accurate dating in the deep basins is a necessary step to follow.

Acknowledgments Seismic data 973G were acquired by GMGS using vessel "Tanbo", and lines ABC, DE, and FG were acquired with vessel "Shiyan-2" by SCSIO. We thank the officers and crew of these vessels for their contributions. Appreciations also go to Jialin Wang, Jiansheng Wu, and Huanjiang Chen for their support. GMT (Wessel and Smith 1995) and USGS potential field software (Phillips 1997) were used in mapping and data processing. This research is funded by Chinese Natural Science Foundation (Grants 40876022, 40776026, 40504016 and 40621063), and by National Basic Research Program of China (973 Program) (Grant 2007CB411702).

References

Agarwal BNP, Shaw RK (1996) Comment on "An analytic signal approach to the interpretation of total field magnetic anomalies" by Shuang Qin. Geophys Prospect 44:911–914. doi:10.1111/j.1365-2478.1996.tb00180.x

Atchuta Rao D, Ram Babu HV, Sanker Narayan PV (1981) Interpretation of magnetic anomalies due to dikes: the complex gradient method. Geophysics 46:1572–1578. doi:10.1190/1.1441164

Blakely RJ (1996) Potential theory in gravity and magnetic applications. Cambridge University Press, Cambridge, pp 1–464

Blakely RJ, Simpson RW (1986) Approximating edges of source bodies from magnetic or gravity anomalies. Geophysics 51:1494–1498. doi:10.1190/1.1442197

Briais A, Patriat P, Tapponnier P (1993) Updated interpretation of magnetic anomalies and seafloor spreading stages in the South China Sea: implications for the tertiary tectonics of Southeast Asia. J Geophys Res 98:6299–6328. doi:10.1029/92JB02280

Briggs IC (1974) Machine contouring using minimum curvature. Geophysics 39:39–48. doi:10.1190/1.1440410

Clift P, Sun Z (2006) The sedimentary and tectonic evolution of the Yinggehai-Song Hong Basin and the southern Hainan margin, South China Sea; implications for Tibetan uplift and monsoon intensification. J Geophys Res 111. doi:10.1029/2005JB004048 doi:10.1029/2005JB004048

Deschamps AE, Lallemand SE, Collot J-Y (1998) A detailed study of the Gagua ridge: a fracture zone uplifted during a plate reorganisation in the Mid-Eocene. Mar Geophys Res 20:403–423. doi:10.1023/A:1004650323183

Dyment J, Arkani-Hamed J (1992) Spreading-rate-dependent magnetization of the oceanic lithosphere inferred from the anomalous skewness of marine magnetic anomalies. Geophys J Int 121:789–804. doi:10.1111/j.1365-246X.1995.tb06439.x

Geological Survey of Japan and Coordinating Committee for Coastal and Offshore Geoscience Programmes in East and Southeast Asia (CCOP) (1996) Magnetic anomaly map of East Asia 1:4,000,000 CD-ROM version, digital geoscience map 2 (P-1)

Hayes DE, Nissen SS (2005) The South China Sea margins: implications for rifting contrasts. Earth Planet Sci Lett 237:601–616. doi:10.1016/j.epsl.2005.06.017

Hsu S-K, Sibuet J-C (1995) Is Taiwan the result of arc-continent or arc-arc collision? Earth Planet Sci Lett 136:315–324. doi:10.1016/0012-821X(95)00190-N

Hsu S-K, Sibuet J-C, Shyu C-T (1996) High-resolution detection of geological boundaries from potential-field anomalies: an enhanced analytic signal technique. Geophysics 61:373–386. doi:10.1190/1.1443966

Hsu S-K, Liu C-S, Shyu C-T, Liu S-Y, Sibuet J-C, Lallemand S, Wang C-S, Reed D (1998) New gravity and magnetic anomaly maps in the Taiwan–Luzon region and their preliminary interpretation. Terrestrial. Atmos Ocean Sci 9:509–532

Hsu S-K, Yeh Y-C, Doo W-B, Tsai C-H (2004) New bathymetry and magnetic lineations identifications in the northeasternmost South China Sea and their tectonic implications. Mar Geophys Res 25:29–44. doi:10.1007/s11001-005-0731-7

Huang C-Y, Xia K-Y, Yuan PB, Chen P-G (2001) Structural evolution from Paleogene extension to latest miocene-recent arc-continent collision offshore Taiwan: comparison with on land geology. J Asian Earth Sci 19:619–639. doi:10.1016/S1367-9120(00)00065-1

Jin Q et al (1989) Geology and hydrocarbon resources of the South China Sea (in Chinese). Geological Press, Beijing, p 417

Jin Z, Xu S, Li Z (2002) Inversion of heterogeneous magnetism for seamounts in the South China Sea (in Chinese). J Ocean Univ Qingdao 32:926–934

Johnson HP, Carlson RL (1992) Variation of sea floor depth with age: a test of models based on drilling results. Geophys Res Lett 19:1971–1974. doi:10.1029/92GL01946

Lee T-Y, Tang C-H, Ting J-S, Hsu Y-Y (1993) Sequence stratigraphy of the Tainan basin, offshore southwestern Taiwan. Petrol Geol Taiwan 28:119–158

Li X (2006) Understanding 3D analytic signal amplitude. Geophysics 71:L13–L16. doi:10.1190/1.2184367

Li Q, Jian Z, Li B (2004) Oligocene-Miocene planktonic foraminifer biostratigraphy, Site 1148, Northern South China Sea. In: Prell WL, Wang P, Blum P, Rea DK, Clemens SC (eds) Proceedings of the ocean drilling program, scientific results 184, 1–26 (Online)

Li C-F, Zhou Z, Li J, Chen H, Geng J, Li H (2007a) Precollisional tectonics and terrain amalgamation offshore southern Taiwan: characterizations from reflection seismic and potential field data. Science in China, series D. Earth Sci 50:897–908

Li C-F, Zhou Z, Li J, Hao H, Geng J (2007b) Structures of the northeasternmost South China Sea continental margin and ocean basin: geophysical constraints and tectonic implications. Mar Geophys Res 28:59–79. doi:10.1007/s11001-007-9014-9

Li C-F, Zhou Z, Hao H, Chen H, Wang J, Chen B, Wu J (2008) Late Mesozoic tectonic structure and evolution along the present-day northeast South China Sea continental margin. J Asian Earth Sci 31:546–561. doi:10.1016/j.jseaes.2007.09.004

Lin AT, Watts AB, Hesselbow SP (2003) Cenozoic stratigraphy and subsidence history of the South China Sea margin in the Taiwan region. Basin Res 15:453–478. doi:10.1046/j.1365-2117.2003.00215.x

Mohan NL, Anand Babu L (1995) An analysis of 3-D analytic signal. Geophysics 60:531–536. doi:10.1190/1.1443790

Nabighian MN (1972) The analytic signal of two-dimensional magnetic bodies with polygonal cross-section—its properties and use for automated anomaly interpretation. Geophysics 37:507–517. doi:10.1190/1.1440276

Nabighian MN (1974) Additional comments on the analytic signal of two dimensional magnetic bodies with polygonal cross-section. Geophysics 39:85–92. doi:10.1190/1.1440416

Nabighian MN (1984) Toward a three-dimensional automatic interpretation of potential field data via generalized Hilbert transforms—fundamental relations. Geophysics 49:780–786. doi:10.1190/1.1441706

Ofoegbu CO, Mohan NL (1990) Interpretation of aeromagnetic anomalies over part of southeastern Nigeria using three dimensional Hilbert transformation. Pure Appl Geophys 134:13–29. doi:10.1007/BF00878077

Pautot G, Rangin C, Briais A, Tapponnier P, Beuzart P, Lericolais G, Mathieu X, Wu J, Han S, Li H, Lu Y, Zhao J (1986) Spreading direction in the central South China Sea. Nature 321:150–154. doi:10.1038/321150a0

Phillips JD (1997) Potential-field geophysical software for the PC, version 2.2. Open-file Rep US Geol Surv 97–725

Roest WR, Verhoef J, Pilkington M (1992) Magnetic interpretation using the 3-D analytic signal. Geophysics 57:116–125. doi:10.1190/1.1443174

Ru K, Pigott JD (1986) Episodic rifting and subsidence in the South China Sea. AAPG Bull 70:1136–1155

Salem A, Ravat D, Gamey TJ, Ushijima K (2002) Analytic signal approach and its applicability in environmental magnetic applications. J Appl Geophys 49:231–244. doi:10.1016/S0926-9851(02)00125-8

Shi X, Qiu X, Xia K, Zhou D (2003) Characteristics of surface heat flow in the South China Sea. J Asian Earth Sci 22:265–277. doi:10.1016/S1367-9120(03)00059-2

Sibuet J-C, Hsu S-K, Le Pichon X, Le Formal J-P, Reed D, Moore G, Liu C-S (2002) East Asia plate tectonics since 15 Ma: constraints from the Taiwan region. Tectonophysics 344:103–134. doi:10.1016/S0040-1951(01)00202-5

Taylor B, Hayes DE (1980) The tectonic evolution of the South China Sea. In: Hayes DE (ed) The tectonic and geologic evolution of South Eastern Asian Seas and Islands, I. Geophysical monograph 23. American Geophysical Union, Washington, pp 89–104

Taylor B, Hayes DE (1983) Origin and history of the South China Sea basin. In: Hayes DE (ed) The tectonic and geologic evolution of South Eastern Asian Seas and Islands, II. Geophysical monograph 27. American Geophysical Union, Washington, pp 23–56

Tsai C-H, Hsu S-K, Yeh Y-C, Lee C-S, Xia K (2004) Crustal thinning of the northern continental margin of the South China Sea. Mar Geophys Res 25:63–78. doi:10.1007/s11001-005-0733-5

Turcotte DL, Schubert G (2002) Geodynamics. Cambridge University Press, Cambridge, p 456

Tzeng J (1994) Tertiary seismic stratigraphic analysis of the Tainan basin (in Chinese). M.S. thesis. National Taiwan University, 102 pp

Wang P, Prell WL, Blum P, Arnold EM, Buehring CJ, Chen M-P, Clemens SC, Clift PD, Colin CJG, Farrell JW, Higginson MJ, Jian Z, Kuhnt W, Laj CE, Lauer-Leredde C, Leventhal JS, Li A, Li Q, Lin J, McIntyre K, Miranda CR, Nathan SA, Shyu J-P, Solheid PA, Su X, Tamburini F, Trentesaux A, Wang L (2000) Proceedings of the ocean drill program, Initial Rep 184. College station, ocean drilling program, TX

Wang TK, Chen M-K, Lee C-S, Xia K (2006) Seismic imaging of the transitional crust across the northeastern margin of the South China Sea. Tectonophysics 412:237–245. doi:10.1016/j.tecto.2005.10.039

Wessel P, Smith WHF (1995) New version of the generic mapping tools (GMT) version 3.0 released. Trans Am Geophys Union EOS 76:329. doi:10.1029/95EO00198

Yan P, Deng H, Liu H, Zhang Z, Jiang Y (2006) The temporal and spatial distribution of volcanism in the South China Sea region. J Asian Earth Sci 27:647–659. doi:10.1016/j.jseaes.2005.06.005

Yao B (1995) Characteristics and tectonic significance of the Zhongnan-Liyue fault. Geological research of the South China Sea (in Chinese). Memoir 7:1–14

Yao B, Zeng W, Hayes DE, Spangler S et al (1994) The geological memoir of South China Sea surveyed jointly by China and USA (in Chinese). China University of Geosciences Press, Beijing, p 204